UCRL-JRNL 202197

An Application of the Coda Methodology for Moment-Rate Spectra Using Broadband Stations in Turkey

Tuna Eken[1], Kevin Mayeda[2], Abraham Hofstetter[3], and Rengin Gok[2], Gonca Örgülü[1], and Niyazi Turkelli[1]

1. *Kandilli Observatory and Earthquake Research Institute*
2. *Lawrence Livermore National Laboratory*
3. *Geophysical Institute of Israel*

This paper was submitted to
Geophysical Research Letters

February 2004

U.S. Department of Energy

Lawrence
Livermore
National
Laboratory

An Application of the Coda Methodology for Moment-Rate Spectra Using Broadband Stations in Turkey

Tuna Eken[1], Kevin Mayeda[2], Abraham Hofstetter[3], Rengin Gök[2], Gonca Örgülü[1], and Niyazi Turkelli[1]

1. Kandilli Observatory and Earthquake Research Institute, Bogazici University, Istanbul, Turkey
2. Lawrence Livermore National Laboratory, USA
3. Geophysical Institute of Israel, Lod, Israel

Abstract

A recently developed coda magnitude methodology was applied to selected broadband stations in Turkey for the purpose of testing the coda method in a large, laterally complex region. As found in other, albeit smaller regions, coda envelope amplitude measurements are significantly less variable than distance-corrected direct wave measurements (*i.e.*, L_g and surface waves) by roughly a factor 3-to-4. Despite strong lateral crustal heterogeneity in Turkey, we found that the region could be adequately modeled assuming a simple 1-D, radially symmetric path correction for 10 narrow frequency bands ranging between 0.02 to 2.0 Hz. For higher frequencies however, 2-D path corrections will be necessary and will be the subject of a future study. After calibrating the stations ISP, ISKB, and MALT for local and regional distances, single-station moment-magnitude estimates (M_w) derived from the coda spectra were in excellent agreement with those determined from multi-station waveform modeling inversions of long-period data, exhibiting a data standard deviation of 0.17. Though the calibration was validated using large events, the results of the calibration will extend M_w estimates to significantly smaller events which could not otherwise be waveform modeled due to poor signal-to-noise ratio at long periods and sparse station coverage. The successful application of the method is remarkable considering the significant lateral complexity in Turkey and the simple assumptions used in the coda method

Introduction

Local and regional coda envelopes are generally thought to be composed of scattered waves that sample some volume surrounding the earthquake source. The first and simplest model to describe the coda was the single-scattering model of Aki (1969) where the volume

sampled is an ellipsoid with the station and source at the foci. A number of observational studies have shown that the volume averaging of the coda waves samples the entire focal sphere and renders them virtually insensitive to any source radiation pattern effect, in contrast to direct waves (*e.g.,* Aki, 1969; Aki and Chouet, 1975; Rautian and Khalturin, 1978). Since the earliest studies on coda, advances in the theoretical background of coda generation and empirical observations have been the subject of extensive study during the last several decades and is reviewed thoroughly by Sato and Fehler (1998).

Mayeda and Walter (1996) studied the seismic source parameters such as energy, moment, and apparent stress drop by using amplitude measurements derived from narrowband coda envelopes for earthquakes in the western United States. More recently Mayeda *et al.* (2003) developed a completely empirical calibration method for obtaining stable seismic source moment-rate spectra derived from local and regional coda envelopes using broadband stations. Their empirical method accounts for path, *S*-to-coda transfer function, site effect, and any distance-dependent changes in coda envelope shape for frequencies ranging between 0.02 and 8.0 Hz.

In the current study we apply the method of Mayeda *et al*. (2003) to the large and tectonically complex region of Turkey, a laterally heterogeneous region that experiences intensive seismic activity (*e.g*.,Bozkurt, 2001; Barka and Kadinsky-Cade, 1988), responsible for numerous destructive earthquakes. However, since the method assumes a simple 1-D radially symmetric path correction, this study region was a good test of the hypothesis that the coda averages over lateral crustal complexity as well as source heterogeneity (*e.g.,* source radiation pattern and directivity).

Data

The Kandilli Observatory and Earthquake Research Institute (KOERI), Bogaziçi University, Turkey, operates a nationwide seismic network for monitoring the seismic activity in and around Turkey. Magnitude calculation plays an important role in KOERI's activities and currently they report duration magnitude (M_d), local magnitude (M_L), and moment magnitude (M_w). In this study, we calibrated three broadband stations, ISKB, ISP, and MALT (Figure 1) for coda-derived moment magnitudes, M_w(coda) and compare against independent moments. We selected over 250 earthquakes recorded at three broadband stations, spanning a distance range of roughly 30 to 1400 km that generally samples the entire country of Turkey (Figure 1). The majority of these events were used to calibrate the coda

envelope shapes and derive path corrections. Of these, 88 events had independent seismic moment estimates that were previously derived from long-period waveform modeling. Approximately 15 of these events were used to derive frequency-dependent site and *S*-to-coda transfer function corrections that transformed the path-corrected coda spectra to an absolute scale. The remaining events were used to validate our calibration procedure by comparing our single-station M_w estimates with those derived from waveform modeling.

Method

We formed $\log_{10}$ averaged envelopes from the two horizontal components for 10 narrow frequency bands ranging between 0.02 Hz to 2.0 Hz (see also Mayeda *et al*., 2003). The coda envelopes for each frequency band can be idealized with the following equation,

$$A_c(f, t, r) = W_o(f) \cdot T(f) \cdot P(r, f) \cdot H(t - t_s) \cdot (t - t_s)^{-\gamma(r)} \exp\left[-b(r) \cdot (t - t_s)\right] \qquad (1)$$

where f is the center frequency, r is the epicentral distance in kilometers, t is the time in seconds from the origin time, t_s is the *S*-wave travel time in seconds, W_o represents the *S*-wave source, T represents the *S*-to-coda transfer function and site effects, P includes the effects of geometrical spreading and attenuation, H is the Heaviside step function, $\gamma(r)$ and $b(r)$ are the distance-dependent coda shape factors that controls the coda envelope shape. However for the purpose of generating synthetics we set W, T, and P to unity. Following the methodology outlined in Mayeda *et al*., (2003), the coda shape parameters and velocity of the peak S/L_g-wave arrival were fit using the form of a hyperbola, [*e.g.*, $b(r) = b_0 - \frac{b_1}{b_2 + r}$] and are listed in Table 1.

Unlike direct waves, the local to near-regional coda appears to be homogeneously distributed in the crust behind the expanding direct wave front and thus requires a different formulation for the attenuation. We demonstrate this with our data using two events that are both well recorded at stations ISP and ISKB. The first event is located only 50 km from ISP but nearly 400 km from ISKB, yet the coda envelopes at 0.1-0.2 Hz are roughly the same level immediately following the direct waves which differ by nearly 2 orders of magnitude (see Figure 2). The second event shows the reciprocal case, and is located much closer to ISKB and yet again, the coda levels are the same, in sharp contrast to the direct waves. From

this observation we expect that after path calibration the corresponding coda synthetics to mimic this behavior. In the following we describe how we derive path corrections starting from coda synthetics generated from the coda shape parameters listed in Table 1. Figure 3a shows examples of uncorrected synthetics (f = 0.1-0.2 Hz) for a unit source (*i.e.,* W=1) at a range of distances. We see that the coda synthetics do not have the same amplitude level, thereby revealing a built-in distance dependence, a result due to $\gamma(r)$ and $b(r)$ changing in the first several hundred kilometers in this example. In contrast, if the coda shape parameters were constant, the envelopes would be identical in both shape and amplitude level at all distances. This distant-dependent bias however, will be accounted for in our path calibration procedure. For each narrowband envelope in our dataset, raw coda amplitudes were determined by generating synthetics at the appropriate distance and using a source of unity then DC shifting using an L-1 norm to fit the observed envelope. The amount of the DC shift is the non-dimensional raw coda amplitude. Next, we use the following empirical equation for coda path correction of Mayeda *et al*., (2003).

$$P(r,f) = \left[1 + \left(\frac{r}{p_2} \right)^{p_1} \right]^{-1} \tag{2}$$

Using common recordings at each station pair, we then grid searched over p_1 and p_2 and tabulated the interstation scatter for each frequency band. The choice of frequency-dependent path correction for the entire region was based upon the path parameters p_1 and p_2 which gave the lowest average interstation standard deviation between station pairs (see Table 1). Figure 3b shows an example of the error surface for path calibration for the average of all 3 possible pairs for the case of f = 0.1-0.2 Hz. With path parameters determined, we can transform the synthetics in Figure 3a to path-corrected envelopes that also account for the distant-dependent bias. The resultant calibrated synthetics exhibit similar coda envelope levels irrespective of distance, in good agreement with the example data shown in Figure 2. After applying the distance corrections to all the raw coda amplitudes we checked the consistency of distance-corrected coda amplitude measurements for common events observed at a station pair. In general, the interstation standard deviation ranged between 0.07 and 0.15 (*e.g.,* Figure 4a) whereas the scatter for distance-corrected L_g and surface waves resulted in an interstation scatter of 0.27-0.45, roughly a factor of 3-to-4 larger (*e.g*., Figure 4b). These results confirm our initial hypothesis that the coda can effectively average over the effects of both source and path heterogeneity.

Results

Although the coda amplitudes are corrected for frequency-dependent path effects, they still carry the *S*-to-coda transfer function as well as site effects and must be removed in order to obtain a moment-rate spectrum that has absolute units (*e.g.*, dyne-cm). We used the moment calibration and empirical Green's function procedure outlined in Mayeda *et al*. (2003), which uses a handful of independently derived seismic moments to tie the low frequency (f < ~0.7 Hz) coda amplitudes to an absolute scale and smaller events as empirical Green's functions to derive corrections for the higher frequencies. In our case, we chose roughly 15 events that had independent moment estimates ranging between $3.9 < M_{\mathbf{w}} < 6.5$ to derive the "site-transfer" corrections (*i.e*., combined site effect and *S*-to-coda transfer function corrections). These values are also listed in Table 1. Next, we applied the path and site-transfer corrections to all the raw coda amplitude data to form moment-rate spectra. Figure 5a demonstrates the consistency between the coda-derived source spectra for earthquakes recorded at the three stations.

We validate our source calibration by comparing against independent seismic moment estimates of roughly 70 earthquakes (~$4.0 < M_w < 7.4$) that generally sampled the entire country of Turkey (see Figure 1). In addition to seismic moment tensors performed in this study, we also took estimates from Örgülü and Aktar (2001) as well as those from the Harvard CMT catalog. For events recorded at multiple stations, their coda-based source spectra were virtually identical, confirming our path and site corrections. Using the low frequency levels of the source spectra, seismic moment values were determined by averaging the measurements of the two lowest frequencies. Next, the moment magnitudes, M_w(coda), were estimated from the following, $M_w = 2/3\log_{10}(M_o) - 10.73$ (Hanks and Kanamori, 1979). Figure 5b shows that the single-station M_w(coda) estimates are in excellent agreement with M_w(waveform), with a data standard deviation of only 0.17 magnitude units.

As a final validation, we have also computed M_w(coda) of several recent earthquakes (see Figure 1) and the results agree very well with waveform modeled results using the long-period waveform modeling approach of Dreger and Helmberger (1993). These include the M_w(coda) 6.3 Pülümür earthquake on January 27, 2003; the M_w(coda) 5.7 Urla earthquake on April 10, 2003; the M_w(coda) 6.4 Bingöl earthquake on May 1, 2003; and the M_w(coda) 4.7 Bandirma earthquake on June 9, 2003.

Discussion and Conclusion

This study represents a successful application of the empirical coda methodology to a broad and tectonically complex region. We summarize our findings as follows: (1) For each frequency band ranging between 0.02 to 2.0-Hz the region was well-fit using a homogeneous, radially symmetric attenuation model despite the lateral tectonic complexity; (2) Single-station M_w(coda) agrees with multi-station inversions for M_w; (3) Coda envelope amplitude measurements are significantly less variable than distance-corrected direct wave measurements (*i.e.*, L_g and surface waves) by roughly a factor 3-to-4; (4) We can use the current calibration parameters to compute M_w(coda) for events that are too small to be waveform modeled as well as events with poor station coverage.

The interstation scatter of distance-corrected coda amplitudes varies from 0.07 to 0.15 in a frequency range between 0.02 and 2.0-Hz, in good agreement with results obtained from previous applications of the methodology to the western United States, Italian Alps, and Dead Sea Rift regions (*e.g.,* Mayeda and Walter, 1996; Malagnini *et al*., 2003, Morasca *et al.*, 2003, Mayeda *et al.,* 2003). We obtained additional validation by computing source spectra of 4 recent large earthquakes such as the M_w(coda) 6.3 Pülümür earthquake on January 27, 2003; the M_w(coda) 5.7 Urla earthquake on April 10, 2003; the M_w(coda) 6.4 Bingöl earthquake on May 1, 2003; and the M_w(coda) 4.7 Bandirma earthquake on June 9, 2003. Our plan is to incorporate these calibrations into a newly developed SAC command that will automatically compute stable, single-station estimates of coda-derived source spectra, moment, and radiated energy for use by KOERI. In addition, it is possible to extend the calibration to other broadband stations in the region by simply deriving empirical site effect corrections for the new stations and using the path corrections and coda shape parameters from the current study.

Acknowledgements

We wish to thank Ms. Jennifer O'Boyle for software development and Mr. Steve Jarpe for modifications to the "coda" command in SAC. This research was supported by the U.S. Department of Energy under project number ROA01-32-LLNL. This work was performed under the auspices of the U.S. Department of Energy by the University of California, Lawrence Livermore National Laboratory under contract No. W-7405-Eng-48. This is LLNL contribution UCRL……

References

Aki, K. (1969). Analysis of seismic coda of local earthquakes as scattered waves, *J. Geophys. Res*., 74, 615-631.

Aki, K. and B. Chouet (1975). Origin of coda waves: source, attenuation and scattering effects, *J. Geophys. Res*. **80**, 3322-3342.

Barka, A. A. and Kadinsky-Cade, K. (1988). Strike-slip fault geometry in Turkey and its influence on earthquake activity. *Tectonics*. 7, 663-684

Bozkurt, E., (2001), Neotectonics of Turkey, Geodinamica Acta, 14, 3-30 (Special Issue).

Dreger, D. S. and D. V. Helmberger (1993). Determination of source parameters at regional distances with single station or sparse network data, *J. Geophys. Res*. **98**, 8107-8125.

Hanks, T. C. and H. Kanamori (1979). A moment magnitude scale, *J. Geophys. Res*., 84, 2348-2350.

Malagnini, L., K. Mayeda, A. Akinci, and P.L. Bragato (2003). Estimating absolute site effects, submitted to *Bull. Seism. Soc. Am*..

Mayeda, K., and W. R. Walter (1996). Moment, energy, stress drop, and source spectra of western United States earthquakes from regional coda envelopes, *J. Geophys. Res*., 101, 11195-11208.

Mayeda, K., A. Hofstetter, J. O'Boyle, W. R. Walter (2003). Stable and transportable regional magnitudes based on coda-derived moment-rate Spectra, *Bull. Seism. Soc. Am*., 93, 224-239.

Morasca, P., K. Mayeda, L. Malagnini, and W.R. Walter (2003). Coda-derived source spectra, moment magnitudes, and energy-moment scaling in the western Alps, submitted to *Geophy. J. Int.*.

Örgülü, G., and M. Aktar (2001). Regional Moment Tensor Inversion for Strong Aftershocks of the August 17, 1999 Izmit Earthquake (M_W-7.4), *Geophys. Res. Lett*., 28, 371-374.

Rautian, T. G. and V. I. Khalturin (1978). The use of the coda for the determination of the earthquake source spectra, *Bull. Seism. Soc. Am*. **68**, 923-948.

Sato, H. and Fehler, M. (1998). Seismic wave propagation and scattering in the heterogeneous earth, AIP Press, New York, Modern Acoustics and Signal Processing.

Figure Captions

Figure 1. Map showing the epicentral distribution of events and stations used in this study. Gray circles represent earthquakes used in the coda calibration procedure. Red squares represent ground-truth earthquakes for which we have independent moment magnitudes and blue stars represent recent earthquakes used for further validation of the method.

Figure 2. Example coda envelopes at f = 0.1-0.2 Hz demonstrating that the coda energy is homogeneously distributed in the crust. The two largest envelopes correspond to an event that is close to ISP (~50 km) but far from ISKB (~450 km), yet their envelope levels are the same, in contrast to the direct waves. Likewise, the two smaller envelopes are for another event, in this case located ~60 km from ISKB and ~400 km from ISP.

Figure 3. a) Synthetic envelopes at 0.1-0.2 Hz at equal intervals ranging between 50 and 500 km using the coda shape and velocity values listed in Table 1 and a source of unity. Notice that the envelope levels are not the same due to changes in the coda shape parameters as a function of distance; **b)** Average error surface for path parameters p_1 and p_2 derived for

events distributed throughout the region; **c)** Same as (a) but after distance corrections were applied. Notice that the calibrated synthetics have the same behavior as the observed data in Figure 2.

Figure 4. a) Distance-corrected direct waves for common events at station ISKB and ISP for the 0.1-0.2 Hz band; **b)** Distance-corrected coda amplitudes for roughly the same events as in (a) where the standard deviation is a factor of 4 times smaller.

Figure 5. a) Examples of coda-derived source spectra computed at stations ISP, ISKB, and MALT. We note that for those events with multiple station recordings, their source spectra are quite similar between the stations; **b)** Single-station coda-derived moment magnitudes agree with the long-period waveform modeled estimates with a data standard deviation of 0.17.

Table 1 Calibration parameters for Turkey where v_0, v_1, v_2 describe the velocity of the peak *S*-wave arrival; b_0, b_1, b_2 and γ_0, γ_1, γ_2 describe the coda envelope shape, where the parameters describe a hyperbola [*e.g.*, $b(r) = b_0 - \frac{b_1}{b_2 + r}$]; p_1 and p_2 are the path parameters; and the constants for each station represent the correction for the combined effect of site effect and *S*-to-coda transfer function.

Freq (Hz)	v0	v1	v2	b0	b1	b2	γ0	γ1	γ2	p1	p2	ISP	ISKB	MALT
0.02_0.03	3.6	96	31	0.00000	0.30	500	0.4	-100	63	2.8	50	19.0005	19.7013	21.4651
0.03_0.05	3.2	54	32	0.00000	0.28	500	0.4	-44	100	1	50	20.2071	20.656	20.0557
0.05_0.1	3.0	24.0	201	-0.00053	0.00	0	0.3	-60	8	1	50	19.7067	20.292	19.7082
0.1_0.2	2.8	22	87	-0.00105	0.04	500	0.3	-73	101	1.5	50	18.7863	18.9188	18.7996
0.2_0.3	3.05	182	201	-0.00210	0.00	0	0.1	-100	101	2	50	18.7208	18.7192	18.781
0.3_0.5	3.2	110	89	-0.00315	0.08	77	0.1	-75	81	2.2	50	18.4804	18.3134	18.5203
0.5_0.7	3.05	28	11	-0.00525	0.10	500	0.1	-85	101	3.2	150	19.3525	18.7977	19.2576
0.7_1.0	3.15	38	20	-0.00630	0.14	500	0.2	-40	73	3.5	150	19.3048	18.5474	19.0583
1.0_1.5	3.5	172	201	-0.00840	0.18	83	0.1	-85	101	3.5	100	18.8296	17.6436	18.6569
1.5_2.0	3.75	242	200	-0.00470	3.50	266	0.4	-28	101	3.8	150	19.2735	17.838	19.3545

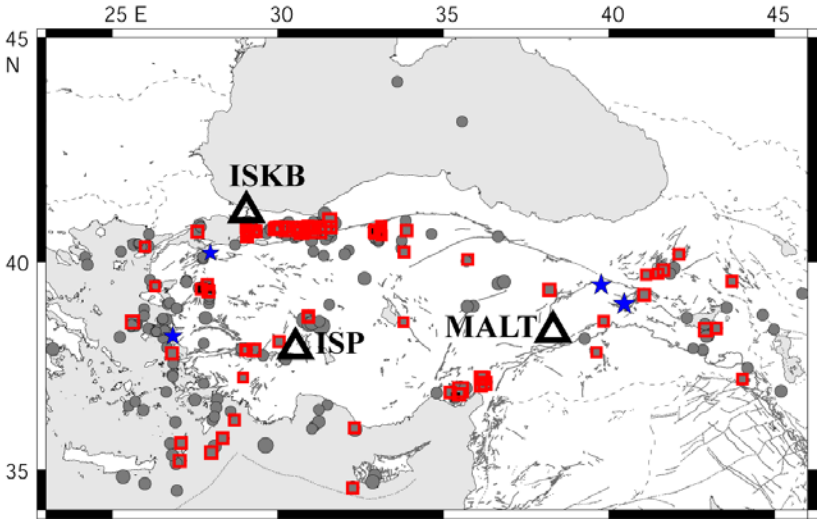

Figure 1

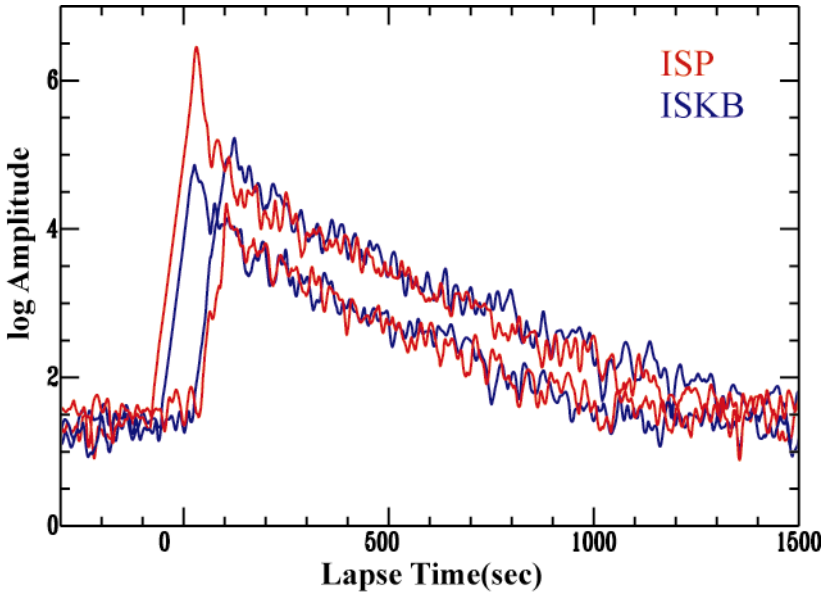

Figure 2

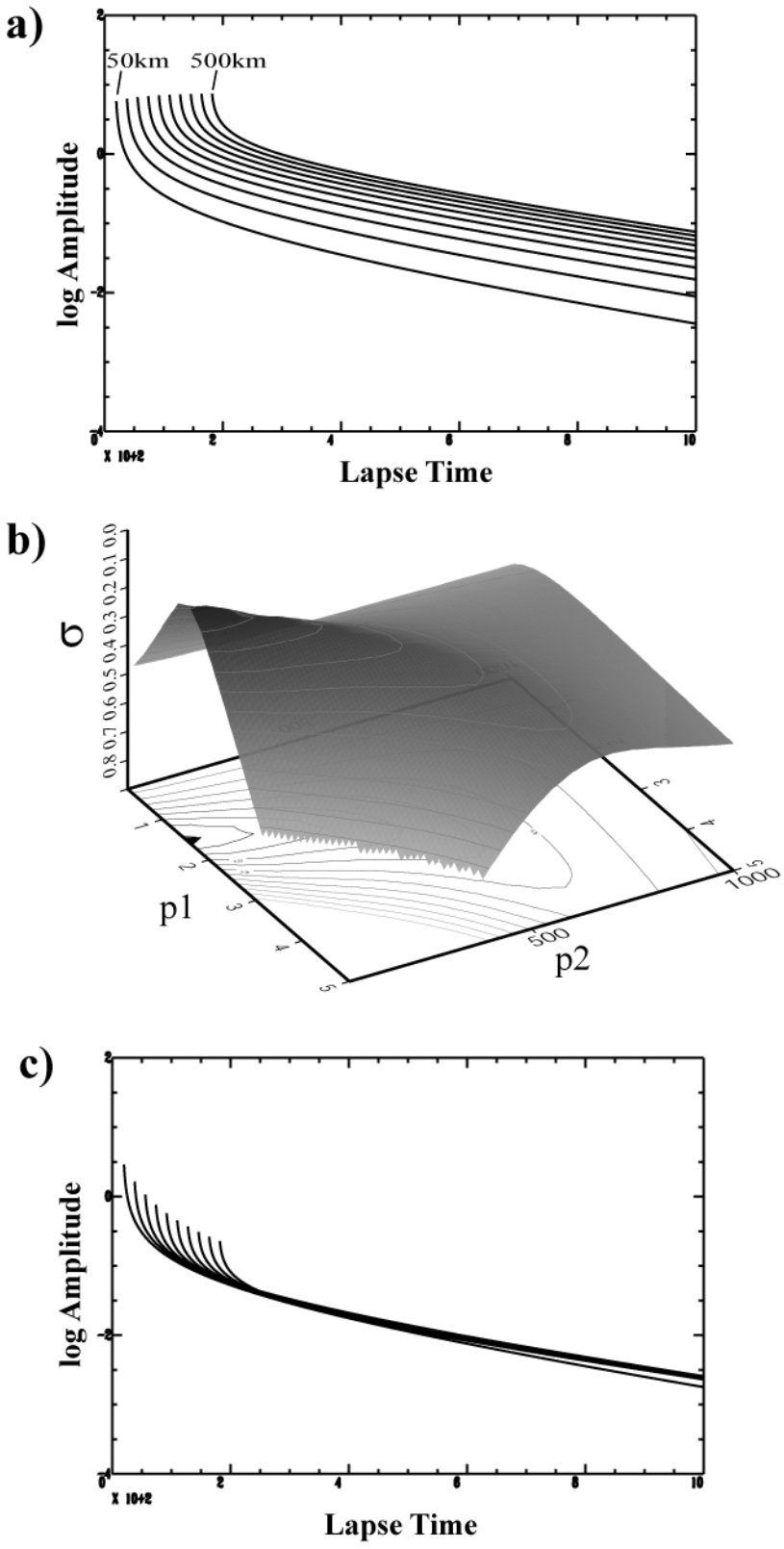
a)
50km
500km
log Amplitude
X 10+2
Lapse Time
b)
σ
p1
p2
c)
log Amplitude
X 10+2
Lapse Time

Figure 3

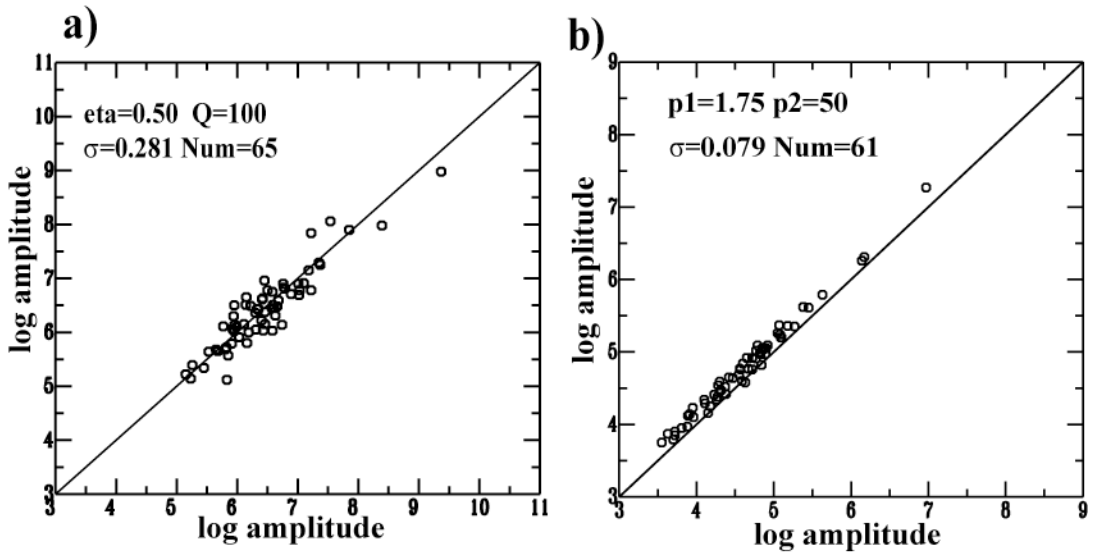
a)
eta=0.50 Q=100
σ=0.281 Num=65
log amplitude
log amplitude
b)
p1=1.75 p2=50
σ=0.079 Num=61
log amplitude
log amplitude

Figure 4

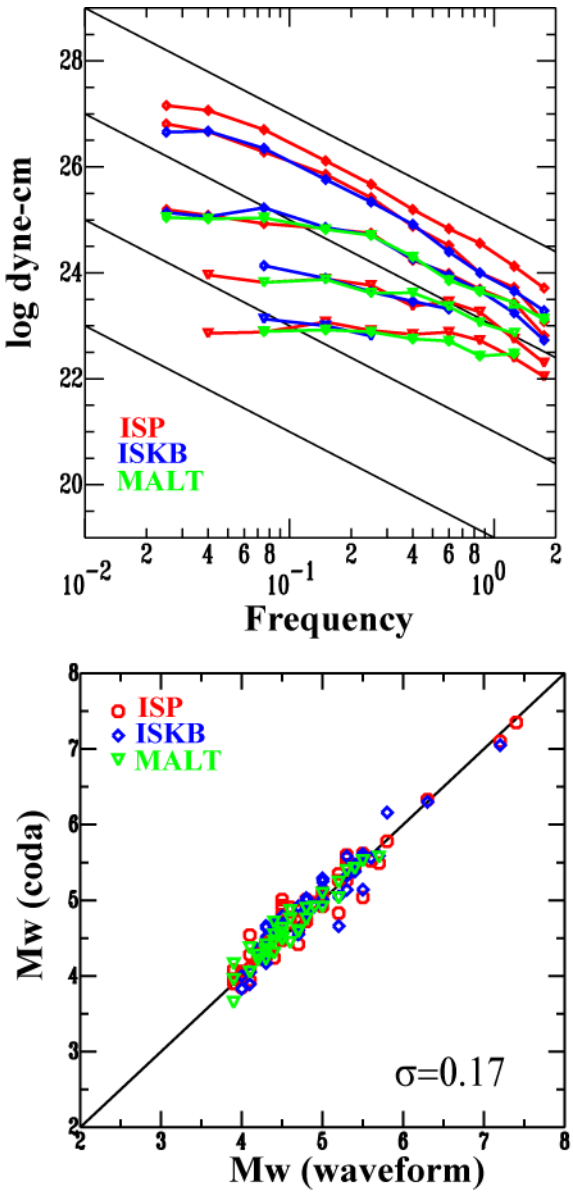
log dyne-cm
28
26
24
22
20
ISP
ISKB
MALT
10^{-2}
10^{-1}
10^{0}
Frequency
Mw (coda)
Mw (waveform)
σ=0.17

Figure 5

University of California
Lawrence Livermore National Laboratory
Technical Information Department
Livermore, CA 94551